Materials & Design 257 (2025) 114542

Contents lists available at ScienceDirect

Materials & Design

journal homepage: www.elsevier.com/locate/matdes

Ceramic-based piezoelectric material reinforced 3D printed polycaprolactone bone tissue engineering scaffolds

Duo Meng [a,1], Yanhao Hou [b,1], Hareem Zubairi [c], Mustafa Tugrul Ucan [a], David A Hall [c], Antonio Feteira [d], Paulo Bartolo [e], Ge Wang [c,*], Weiguang Wang [b,*]

[a] Department of Mechanical and Aerospace Engineering, School of Engineering, Faculty of Science and Engineering, The University of Manchester, Manchester M13 9PL, UK
[b] Department of Mechanical Engineering, School of Engineering, Faculty of Engineering and Physical Sciences, University of Southampton, Southampton SO17 1BJ, UK
[c] Department of Materials, School of Natural Sciences, Faculty of Science and Engineering, The University of Manchester, Manchester M13 9PL, UK
[d] Materials and Engineering Research Institute, Sheffield Hallam University, Sheffield S1 1WB, UK
[e] Singapore Centre for 3D Printing, Nanyang Technological University, Singapore 639798 Singapore

ARTICLE INFO

Keywords:
Bone Tissue Engineering
Piezoelectric Ceramic
Polymer
Scaffold

ABSTRACT

Recent studies confirm the piezoelectricity of human bone, sparking interest in biocompatible and biodegradable piezoelectric scaffold development. These scaffolds mimic native bone by matching its mechanical properties and piezoelectric behaviour i.e., generating local electrical stimulation under mechanical stress, or generating mechanical response under external electrical stimulation, thereby modulating cellular activity, accelerating cell proliferation and differentiation, ultimately speeding up the regeneration process. Although polymer-based piezoelectric materials offer high reproducibility for 3D scaffolds, their piezoelectric performance falls short of ceramic alternatives. While lead zirconate titanate (PZT) exhibits excellent piezoelectric properties, the hazardous nature of lead limits biomedical applications. Consequently, this research proposes novel lead-free $Bi_{1/2}Na_{1/2}TiO_3$-based (BNT) piezoelectric materials, namely, direct piezoelectric ceramics (DPC) (>50 % d_{33} enhancement compared to undoped BNT) and converse piezoelectric ceramics (CPC) (>200 % S_{max} enhancement compared to undoped BNT), with properties optimized for bone tissue engineering (BTE). 3D BTE scaffolds are designed and fabricated considering biocompatible and biodegradable polycaprolactone (PCL) incorporating DPC and CPC as functional fillers. Comparative evaluations against hydroxyapatite (HA), a well-accepted bioceramic for clinical applications, are conducted for surface, mechanical, and biological properties. Results proved the incorporation of both DPC and CPC promotes the mechanical properties (88.6 % enhancement compared to neat PCL) and cell proliferation rate (46.3 % improvement compared to HA). Notably, hybrid scaffolds combining both PCL/DPC and PCL/CPC in a cascade manner also outperformed PCL/HA (by 7.4 %) in osteogenic differentiation, indicating promising potential for future studies.

1. Introduction

Current advancements in bone tissue engineering (BTE) have led to the rapid development of synthetic polymeric scaffolds fabricated by additive manufacturing (AM). These scaffolds are biocompatible and biodegradable, have adequate mechanical properties for critical-sized bone loss regions, being capable of accommodating various types of stimuli, and thus are clinically capable of modulating the process of bone regeneration following scaffold implantation [1,2]. Benefiting from the unique advantage of AM: mass-personalisation, these scaffolds can also be tailored to fit the specific needs of each patient [3]. External electrical stimulation, endogenous electrical fields, and bioelectrical signals are pivotal in regulating cellular behaviour and contributing to bone regeneration [4,5]. Therefore, among the various types of BTE scaffolds, electroactive scaffolds present unique advantages. This is achieved by either imparting the scaffold with electrical conductivity or piezoelectric property, thus transmitting electrical signals and enhancing the physiological electrical environment to promote bone regeneration [6,7].

Electrically conductive materials, such as conductive polymers (e.g., polypyrrole, polyaniline), carbon-based materials (e.g., graphene,

* Corresponding authors.
E-mail addresses: ge.wang@manchester.ac.uk (G. Wang), weiguang.wang@soton.ac.uk (W. Wang).
[1] These authors contributed equally to this work.

https://doi.org/10.1016/j.matdes.2025.114542
Received 30 June 2025; Received in revised form 5 August 2025; Accepted 7 August 2025
Available online 8 August 2025

carbon nanotubes), and metallic nanoparticles, have been employed in scaffold development to enhance the electrical signalling and thus support osteogenic activity [8–10]. However, these materials typically only function as passive conductors, requiring external power sources and offering limited dynamic interaction with the surrounding tissue [11]. Compared with electrically conductive scaffolds that only guide electrical stimulation, the piezoelectric ones present unique piezoelectricity mimicking the natural bone tissue. Generally, they present two-way stimulation generation functions [12]: Direct piezoelectric effect in which scaffold materials generate electrical signals in response to the mechanical stimulation during daily movement. Converse piezoelectric effect in which scaffold materials generate mechanical responses through the application of *ex vivo* electrical stimulation (from a clinician). The research on applying piezoelectric biomaterials to BTE scaffolds has shown an emerging trend. Ceramic-based piezoelectric materials, which benefited from superior piezoelectric properties, have been extensively explored as materials for producing scaffolds [13]. Lead zirconate titanate (PZT) ceramics, as commercial piezoelectric materials, have excellent piezoelectric properties with the direct piezoelectric coefficient (d_{33}) as high as ~ 500 pC/N, but are challenging to use in any tissue engineering applications due to the cytotoxicity of Pb/PbO [14]. Thus, lead-free piezoelectric ceramics such as zinc oxide (ZnO), barium titanate (BT), potassium-sodium niobate (KNN), lithium sodium–potassium niobate (LNKN) have been investigated as promising replacements for PZT [13].

Ceramic-based scaffold tends to present high piezoelectricity [15], it is possible to electrically stimulate osteoblasts in a biomimetic manner during cyclic mechanical loading. However, drawbacks such as mechanical brittleness, difficulty, and low reproducibility in manufacturing, low biocompatibility, and biodegradability have limited their development in BTE applications [16,17]. Thus, considering biocompatible and biodegradable polymeric material as the scaffold base material and using ceramic-based piezoelectric material as functional fillers appears to be a promising route to tackle the challenges. Polycaprolactone (PCL) is an ideal base material for BTE scaffold fabrication due to its ease of processing, desirable biocompatibility, and biodegradability [18–20]. Research on utilising AM for the fabrication of porous polymer/piezoelectric ceramic material scaffolds is limited. Among the few available studies, Salehi Sadati *et al.* developed PCL BTE scaffolds containing BT and HA nanoparticles, which showed promising piezoelectricity and biocompatibility [21]. Similarly, Mancuso *et al.* also developed PCL/HA and PCL/BT scaffolds and compared their performance with the neat PCL scaffold. The results showed that the addition of HA and BT conferred the scaffold with improved mechanical and biological properties [22]. However, the feasibility of combining two types of ceramic-based piezoelectric materials that present direct and converse piezoelectric effects into a single scaffold, in a controllable manner, still needs further investigation. This is due to the lack of understanding of both material development (increasing piezoelectric ceramic biocompatibility without compromising piezoelectric performance) and fabrication technology (accurate and selective multi-material printing). Some recent research explored a variety of electrospun scaffolds incorporating piezoelectric polymer with bioceramic, but they present significant limitations in terms of mechanical performance (due to material blending and manufacturing strategy) and biodegradability [9,23]. These studies also overlooked *in vivo* analysis, haven't systematically studied the effect of direct and/or converse piezoelectric effect on BTE applications, let alone the exploration of combining both.

A promising strategy is the precise, filament-by-filament and layer-by-layer deposition of direct and converse piezoelectric materials separately within the single BTE scaffold, enabled by material-extrusion AM. It minimises the unwanted ceramic dosing, reduces the total amount of non-biodegradable ceramic materials, and increases the biodegradability while allowing the zonal functionality control. This paper presents the first attempt at a combined investigation of developing two lead-free ceramic-based piezoelectric materials and applying them to the AM fabrication of the next-generation BTE scaffolds, considering different loading levels and controllable porous 3D structures. The designed scaffold considers both a single piezoelectric material and direct-converse piezoelectric combinations. Comprehensively, mechanical, chemical, morphological, surface, and *in vitro* biological properties were characterised through a series of experimental validations. Through the comparison with PCL and PCL/HA scaffold, the performance in mechanical and biological perspectives was highlighted, and the feasibility for future *in vivo* research was also evaluated.

2. Materials and methods

2.1. Piezoelectric ceramics synthesis and characterisation

A series of (1-x) $Bi_{1/2}Na_{1/2}TiO_3$-x$KNbO_3$ (x = 0.01–0.09) piezoelectric ceramics was synthesized via solid-state reaction. Briefly, high-purity powders (≥ 99 %) of Na_2CO_3, Bi_2O_3, TiO_2, K_2CO_3, and Nb_2O_5 were weighed stoichiometrically, ball-milled (Megapot, Pilamec Ltd.) for 24 h, dried, and calcined at 900 °C for 2 h. After a second 24-hour ball-milling, the powders were dried, with binder added (10 wt.% PVA) before pressing into 10 mm diameter pellets. To minimise volatilisation of Bi, Na, and K elements, pressed pellets were embedded in the powder of the same composition and sintered at 1140–1200 °C for 3 h in the air with a binder burnout stage at 550 °C for 3 h. The resulting piezoelectric ceramics, designated as direct piezoelectric ceramics (DPC) and converse piezoelectric ceramics (CPC), exhibited ~ 20–25 % volume shrinkage with relative density > 93 %. Samples were ground to 0.5 mm thickness and electroded with silver paste (Sunchemical, UK), fired at 550 °C for 2 h prior to electrical measurements.

Polarisation-electric field (P-E) and strain-electric field (S-E) loops were measured using an aixACCT TF 2000E ferroelectric tester at a frequency of 1 Hz. Microstructural analysis was performed using scanning electron microscopy (Philips XL30, Netherlands) after grinding and polishing. The average grain size was determined using the linear intercept method.

2.2. Scaffold design and fabrication

The synthesized DPC and CPC pellets were crushed into ceramic powders using vibration milling (Megapot, Pilamec Ltd., UK) for 48 h and sieved. The obtained agglomerate size is around 8–10 μm as examined via SEM. PCL (Capa 6500, Ingevity, UK) in the form of 3 mm pellets and hydroxyapatite (HA, Sigma-Aldrich, UK) in the form of < 200 nm particle size nano powder were purchased from the suppliers. PCL-based composite materials containing different concentrations of HA, DPC, or CPC were prepared by a physical melt mixing process (material compositions detailed in Table 1). In summary, the PCL pellets were first heated to 150 °C, with the desired concentration of different materials added and mixed for 30 min to achieve uniform dispersion. Upon cooling to room temperature, the blended materials were then separated into smaller pellets ready for printing. Scaffold fabrication was conducted using a screw-assisted material extrusion additive manufacturing system (3DDiscovery, RegenHU, Switzerland). The fabrication parameters (Table 1) were optimized, allowing for constant control over the topological structure close to the design and high reproducibility. All scaffolds were printed as 12 layers with dimensions of 32.00 × 32.00 × 3.24 mm. The hybrid scaffolds (abbreviated as PCL/DPC/CPC) were fabricated by first printing DPC for 6 layers and then CPC for another 6 layers. All printed scaffolds were tested by thermogravimetric analysis (TGA) to evaluate that both types of functional fillers were effectively incorporated and uniformly dispersed into the polymer matrix at the intended concentrations (as shown in Table 1 and Fig. S1). TGA was carried out on a Q500 instrument (TA Instruments, USA) using approximately 6 ± 1 mg of sample per run. All measurements were conducted under N_2 atmosphere with a flow rate of 90 mL/min. The temperature was ramped from 30 °C to 560 °C at a constant rate of

Table 1
Scaffold design, material composition and processing parameters.

Scaffold type	Abbreviation	Designed material composition	Actual functional filler concentration validated by TGA	Processing parameters
Standard scaffold	PCL/HA-2.5	PCL contains 2.5 wt.% HA	2.71 ± 0.27 wt. %	Nozzle diameter: 330 μm
	PCL/HA-5	PCL contains 5 wt.% HA	4.92 ± 0.14 wt. %	Melting and printing temperature: 90 °C
	PCL/DPC-2.5	PCL contains 2.5 wt.% DPC	2.51 ± 0.10 wt. %	Deposition velocity: 11.8 mm/s
	PCL/DPC-5	PCL contains 5 wt.% DPC	5.00 ± 0.20 wt. %	Screw rotation velocity: 10.8 rpm
	PCL/CPC-2.5	PCL contains 2.5 wt.% CPC	2.51 ± 0.08 wt. %	Fibre diameter: 330 μm
	PCL/CPC-5	PCL contains 5 wt.% CPC	4.98 ± 0.18 wt. %	Fibre lay-up pattern: 0°/90°
Hybrid scaffold	PCL/DPC/CPC-2.5	6 layers PCL contains 2.5 wt.% DPC + 6 layers PCL contains 2.5 wt.% CPC	2.51 ± 0.10 wt. % DPC + 2.51 ± 0.08 wt. % CPC	Layer count: 12 layers
	PCL/DPC/CPC-5	6 layers PCL contains 5 wt.% DPC + 6 layers PCL contains 5 wt.% CPC	5.00 ± 0.20 wt. % DPC + 4.98 ± 0.18 wt. % CPC	Slice thickness: 220 μm

* PCL stands for polycaprolactone; HA stands for hydroxyapatite; Direct piezoelectric ceramics (DPC) stands for 0.98BNT-0.02KN and converse piezoelectric ceramics (CPC) stands for 0.93BNT-0.07KN.

10 °C/min. The ceramic content within the composites was estimated by evaluating the mass loss observed during thermal degradation.

2.3. Scaffold surface hydrophilicity characterization

KRÜSS DSA 100 (KRÜSS Instruments, Germany) drop shape analyser system was utilized to assess the scaffold's surface hydrophilicity. Prior to each measurement, the 32.00 × 32.00 × 3.24 mm scaffold was rinsed with deionized water and dried at room temperature for 24 h. 1.7 μL of deionized (DI) water was dropped onto the surface of the scaffolds by a micro liquid dispenser (Hamilton, USA) with the needle located approximately 5 mm above the surface. All measurements were conducted at room temperature. The droplet deposition process was recorded, and the water contact angle (WCA) was determined from the image captured after the droplet stabilized (within approximately 5 s), utilizing the Drop Shape Analysis (KRÜSS Instruments, Germany) software with the sessile drop method.

2.4. Scaffold mechanical characterization

Uniaxial mechanical compression tests were performed to evaluate all produced scaffolds' compressive modulus and strength. Specimens were prepared as blocks measuring 3.00 × 3.00 × 3.24 mm according to the ASTM D1621-16 standard [24]. The INSTRON 3344 singl-column table frame system (Norwood, USA), equipped with a 100 N load cell, was utilized. All experiments were conducted in dry conditions, considering the 0.5 mm/min compression rate and 0.2 mm/mm (20 %) strain limit. The force (F) and the corresponding displacement values were registered and converted into engineering stress (σ) and strain (ε). The compressive strength and compressive modulus were subsequently analysed following the methodology outlined by Fiedler *et al.* [25].

2.5. In vitro biological characterization

2.5.1. Cell culture

Human adipose-derived stem cells (hADSCs, StemPro®, Invitrogen, USA) at passages 8–9 were selected for all *in vitro* biological evaluations. Cells were cultivated in T75 flasks (Sigma-Aldrich, UK) using MesenPRO RS™ basal medium (Invitrogen, USA) till 80 % confluency. Prior to cell seeding, all scaffold samples were cut to the appropriate size (7.00 × 8.00 × 3.24 mm) fit 48-well plates (Corning, USA), sterilized with 70 % ethanol, rinsed with phosphate-buffered saline (PBS, Sigma-Aldrich, UK), and left to air-dry overnight. Approximately 2.0 × 10^4 hADSCs were then seeded onto each sample. The cultures were maintained under standard conditions (37 °C, 5 % CO_2, and 95 % humidity), with the culture medium being refreshed every two days throughout the *in vitro* biological assessment.

2.5.2. Cell proliferation

Alamar Blue assay was utilized to assess cell cytotoxicity, proliferation, and viability status on scaffolds at days 1, 3, 5, and 7 post-seeding, using resazurin sodium salt (Invitrogen, USA). At each time point, the cell-seeded scaffolds were transferred to a new 48-well plate, with each well receiving 400 μL of culture medium containing 0.001 % (w/v) resazurin sodium salt. Following a 4-hour incubation period, 150 μL of medium was transferred to a 96-well plate and analysed using a TECAN Infinite 200 plate reader (E_x/E_m = 540/590 nm, Tecan Group Ltd., Switzerland).

2.5.3. Osteogenic differentiation

In order to understand the hADSc osteogenic differentiation result on scaffolds, the enzymatic activity of Alkaline Phosphatase (ALP) was assessed using the SensoLYTE® pNPP Alkaline Phosphatase assay kit (AnaSpec, USA). The calcium deposition process was evaluated using Alizarin Red-S (ARS, Sigma-Aldrich, UK) staining. Generally, all cell-seeded scaffolds were first cultured in proliferation medium (MesenPRO RS™ basal medium) for 7 days, changed to osteogenic differentiation medium (StemPro™ Osteogenesis Differentiation Kit), and continued the culture work for the additional 3, 7, and 14 days before each evaluation. The differentiation time points are noted as 7 + 3, 7 + 7, and 7 + 14 days. For ALP, at each time point, the cultured scaffolds were first rinsed with PBS and assay buffer, transferred to 15 mL centrifuge tubes containing 0.8 mL of assay buffer supplemented with 0.2 % (v/v) Triton X-100 (Sigma-Aldrich, UK). After vertexing for 1 min, sonication for 2 min, storing at −80 °C for 15 min, and finally thawing at ambient temperature, all samples were centrifuged at 2500g for 10 min at 4 °C. To assess protein phosphatase activity, 50 μL of top supernatants were extracted from each tube and mixed with 50 μL of p-nitrophenyl phosphate. After incubating at room temperature for 1 h, a stop solution was added to each well, and the absorbance was measured at 405 nm using a TECAN Infinite 200 plate reader. For ARS, at each time point, scaffolds underwent a series of steps: washing and immersion in a 10 % neutral formaldehyde solution (Sigma-Aldrich, UK) for 15 min, rinsing with DI water, application of 0.2 % (w/v) ARS staining dye, and incubation at ambient temperature for 40 min. Subsequently, the scaffolds were washed with DI water, treated with 0.8 mL of 10 % acetic acid, and transferred into 15 mL centrifuge tubes. The scaffolds were incubated for 30 min with mild vibration, then heated to 85 °C for 10 min, followed by a 5 min cooling period on ice. Following centrifugation at 2500g for 15 min, 400 μL of supernatant was collected and mixed with 150 μL of 10 % ammonium hydroxide to adjust the pH to 4.1–4.5. The absorbance at 405 nm was measured using a TECAN Infinite 200 plate reader.

2.5.4. Bioimaging

Both confocal microscopy and SEM imaging were employed to further assess cell qualitative adhesion, spreading, proliferation, and differentiation status. The cell-seeded scaffolds were fixed at the time points day 3 and day 7 for proliferation, and day 7 + 7 and day 7 + 14 for

differentiation. Briefly, samples containing cells were fixed using a 10 % paraformaldehyde solution (Sigma-Aldrich, UK) for 40 min, rinsed three times with phosphate-buffered saline (PBS), and subsequently immersed in PBS with 0.1 % Triton X-100 (Sigma-Aldrich, UK) for 7 min. After twice PBS rinses, the samples were treated with PBS containing 7 % fetal bovine serum (FBS, Sigma-Aldrich, UK) and incubated for 30 min at ambient temperature. Thereafter, cellular actin was stained with Alexa Fluor™ 594 Phalloidin (Invitrogen, USA) at a 1:400 dilution for 45 min in the dark, as recommended by the manufacturer. Following two further PBS rinses, cell nuclei were stained with 4′,6-Diamidino-2-phenylindole dihydrochloride (DAPI) (Invitrogen, USA) at the recommended concentration (1:800). A Leica SP8 LIGHTNING confocal microscope (Leica, Germany) was utilized to capture confocal images.

For SEM analysis, all cell-seeded scaffold samples were initially treated with a 10 % glutaraldehyde solution (Sigma-Aldrich, UK) for 45 min at ambient temperature, followed by a PBS rinse. The samples were then dehydrated using a graded ethanol series (50 %, 70 %, 80 %, 90 %, and 100 %), with each step lasting 10 min. Subsequently, they were sequentially immersed in a solution composed of 50 % ethanol and 50 % hexamethyldisilazane (HMDS, Sigma-Aldrich, UK), followed by pure HMDS and finally air-dried to ensure complete HMDS removal. Prior to imaging, a 6 nm layer of gold–palladium (80:20) was sputter-coated onto the samples using a Q150T ES sputter coater (Quorum Technologies, UK). Imaging was performed using a TESCAN MIRA3 system (TESCAN, Czech) at an accelerating voltage of 2 kV. Additionally, Energy Dispersive X-ray Spectroscopy (EDX) was conducted with the same system at 15 kV, and the data were analysed using AZtec software (Oxford Instrument, UK).

Further analysis of the calcium area on differentiated samples was conducted on the obtained SEM images. The images were processed by the MATLAB (MathWorks, USA) code created through the image processing toolbox. When extracting objects from binary images, only circularity values higher than 0.51 were considered as calcium area, and calcium within the scaffolds was captured via area filtering. The extracted calcium shape was then processed by MATLAB code to calculate the corresponding area. The MATLAB code was attached as supplementary material Code S1.

2.6. Data analysis

All investigations were conducted with at least three scientific replicates, and the experimental data were provided as the mean value and standard deviation. The data analysis was first carried out using Shapiro-Wilk and Levene's tests through OriginLab (OriginLab Corporation, USA) and followed by one-way analysis of variance (one-way ANOVA) with *post hoc* Tukey's test. Statistical significance was determined at levels of * $p < 0.05$, ** $p < 0.01$, and *** $p < 0.001$.

3. Results and discussions

3.1. Development on the piezoelectric ceramics

3.1.1. Direct piezoelectric ceramics (DPC) characterization

Previous studies have demonstrated the electric field and temperature-induced phase transition behaviour in lead-free $Bi_{1/2}Na_{1/2}TiO_3$ (BNT) based solid solutions between short-range relaxor ferroelectric (RFE) to long-range ferroelectric (FE) phase, as a key optimisation strategy for direct and converse piezoelectric responses [26]. For example, the d_{33} was found to be enhanced by electric field-induced transformation from a pseudo-cubic to a mixed phase of rhombohedral and tetragonal in BNT-$NaNbO_3$ solid solution [27].

The development of the DPC in this study focuses on (1-x) $Bi_{1/2}Na_{1/2}TiO_3$-x$KNbO_3$ (BNT-xKN) ceramics with x = 0.01–0.05. The single pseudo-cubic structure was obtained for all compositions under X-ray diffraction (XRD), as reported previously [28]. Bipolar polarisation-electric field (P-E) loops at 60 kV cm^{-1} of DPC were displayed in Fig. 1(a). For compositions with x = 0.01–0.03, saturated ferroelectric-type P-E loops were obtained with high P_{max} and P_{rem} over 30 μC cm^{-1}, Fig. 1(b), indicating electric field induced irreversible transformation from nonergodic-relaxor to long-range ferroelectric phase. Increasing x concentration to 0.04 and 0.05, constricted P-E loops were observed, suggesting that the phase transition between the relaxor and long-range ferroelectric phase became reversible [29]. It is also noticed that the E_c drops gradually with increasing x content from approximately 55 to 25 kV cm^{-1}. The optimised d_{33} value of poled piezoelectric ceramics, 125

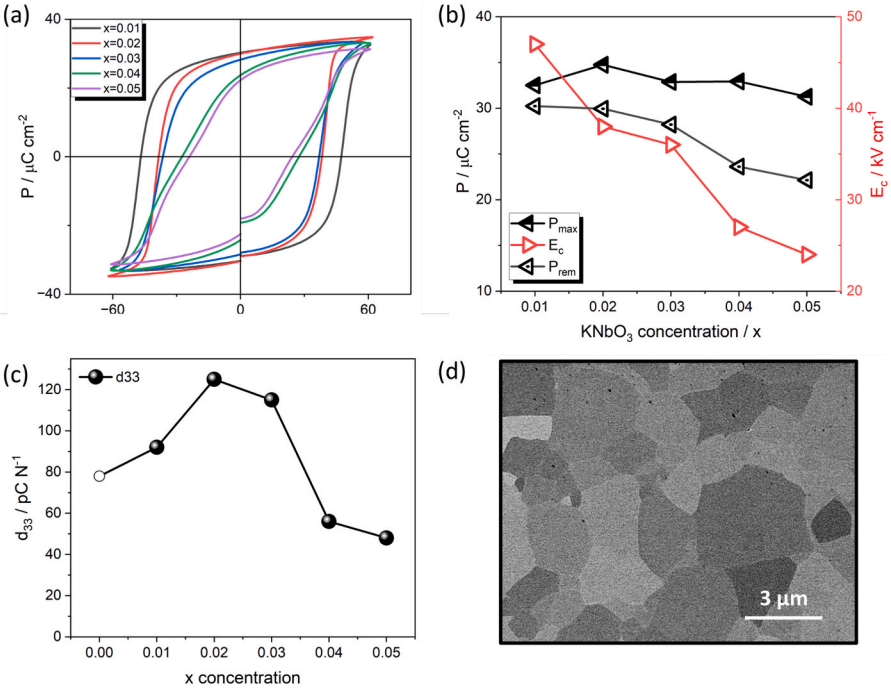

Fig. 1. DPC characterization result. (a) Bipolar ferroelectric P-E hysteresis loops. The changes on the (b) polarisation and coercive field and (c) direct piezoelectric coefficient for DPC. (d) Polished SEM cross-section of the optimal 0.98BNT-0.02KN piezoelectric ceramics.

pC N^{-1}, was found at the composition with x = 0.02 (Fig. 1(c)), with > 50 % enhancement compared to undoped BNT [30]. This value is similar to other BNT-based solid solutions such as BNT-BT [30] and BNT-$NaNbO_3$ [27], however, it is inferior to other lead-free piezoelectrics such as $K_{0.5}Na_{0.5}NbO_3$ [31]. The optimised direct piezoelectric performance originates from irreversible phase transition and subsequent domain switching behaviour, corresponding well with the previous studies on electric field induced structural studies [28]. The average grain size for the optimised composition was found to be 3.2 ± 0.5 μm, as shown in Fig. 1(d). 0.98BNT-0.02KN is thus considered a promising DPC candidate with optimal d_{33} and appropriate grain size for the follow-on study.

3.1.2. Converse piezoelectric ceramics (CPC) characterization

The development of the CPC in this study focuses on (1-x) BNT-xKN ceramics with x = 0.03–0.09. It has been reported that the reversible phase between relaxors (with polar nano regions) and long-range/meso ferroelectrics is a critical characteristic for optimising electrostrain behaviour in BNT-based ceramics [32]. Such behaviour will be explored in this study for the development of the CPC.

Bipolar P-E and strain-field (S-E) loops of CPC at 60 kV cm^{-1} are displayed in Fig. 2(a-c). For compositions with x = 0.04–0.07, constricted P-E loops were obtained, indicating the occurrence of a reversible phase transition between ergodic-relaxor and ferroelectric phases [33]. Both P_{max} and P_{rem} reduce as x increases, Fig. 2(d). For x = 0.03, a ferroelectric butterfly S-E loop was observed, Fig. 2(b), yielding a negative strain of −0.08 % and positive strain of + 0.10 %, corresponding to the long-range ordered ferroelectric phase. With increasing x concentration toward 0.07, the shape of the S-E loop has changed, with negligible negative and enhanced positive strains. Such behaviour has been reported previously in lead-free BNT-based compositions, where maximum positive electrostrain (S_{max}) was effectively enhanced by the reversible transformation between short-range ergodic relaxor and long-range ferroelectric through compositional modification [34]. Here in this study, the enhanced S_{max} (both bipolar and unipolar) of 0.33 %, (equivalent to large-signal converse piezoelectric coefficient d_{33}*) of 550 pm V^{-1}, were obtained at 0.93BNT-0.07KN, Fig. 2(b) and 2(c), realising a significant > 200 % enhancement compared to undoped BNT ceramics [35]. This value is superior to most of the other lead-free piezoelectric ceramics based on $BiFeO_3$ [36], BT [37], and $K_{0.5}Na_{0.5}NbO_3$ [31]. Further increasing x content to 0.09, the electric field is unable to induce any type of meso/long-range FE ordering, thus an electrostrictive-like strain is observed with S_{max} ~ 0.05 %. 0.93BNT-0.07KN is therefore considered a promising CPC candidate with optimal S_{max} for the following investigation.

The P-E loops of piezoelectric (BNT-based) and HA ceramic-loaded PCL scaffolds were also evaluated (Fig. S2). The P_{max} value was found to be relatively low, <0.01 μC cm^{-2}, at an electric field of 10 kV cm^{-1} for the HA ceramic-loaded PCL scaffold. In contrast, P_{max} was enhanced significantly by at least 1 order of magnitude for the BNT-based piezoelectric ceramic-loaded PCL scaffold, desirable for realising piezoelectric activities. The polarisation of PCL/piezoelectric ceramic scaffolds has not been reported in the current literature. However, as the ferroelectric polarisation has a strong correlation to piezoelectric properties, the obtained value in the study can work as an important indicator. A d_{33} of ~ 3 pC/N was reported in PCL/BT composites by Liu *et al.*, however, this was evaluated using dense composite samples rather than porous scaffolds [38]. Further studies on the direct evidence of piezoelectric properties from a PCL/piezoelectric ceramic scaffold will be conducted.

3.2. Scaffold physical characterization

3.2.1. Water contact angle (WCA)

Acellular BTE scaffold requires appropriate surface hydrophilicity to support cell adhesion and proliferation [39]. The results of the WCA measurements are presented in Fig. 3(a), which shows the surface wettability of all fabricated scaffolds (values below 90° indicating hydrophilicity and above 90° indicating hydrophobicity). For BTE scaffolds, studies suggest a contact angle between 40° and 70° is optimal [40–43]. The WCA of the standard PCL scaffold was 90.33 ± 0.32°, but with the addition of ceramic fillers, the WCA dropped significantly, closer to the optimal range. The increase in hydrophilicity is also dependent on the filler concentration. Among all groups, the addition of 5 wt.% CPC presented the most significant impact, reducing the contact

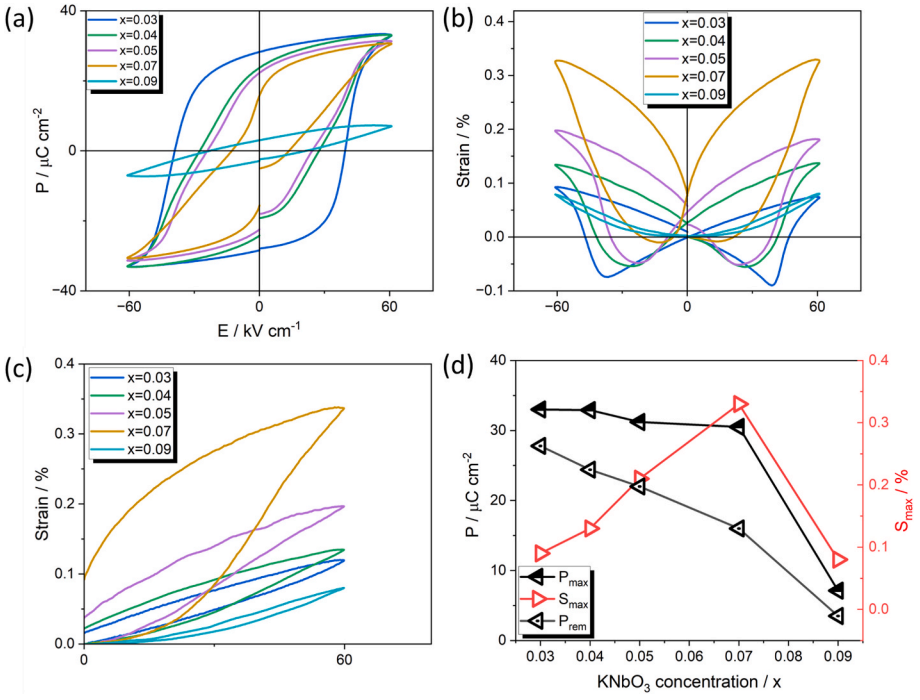

Fig. 2. CPC characterization result. (a) Bipolar P-E loops, (b) Bipolar S-E loops and (c) Unipolar S-E loops of CPC. (d) The changes on polarisation and maximum strain of the CPC.

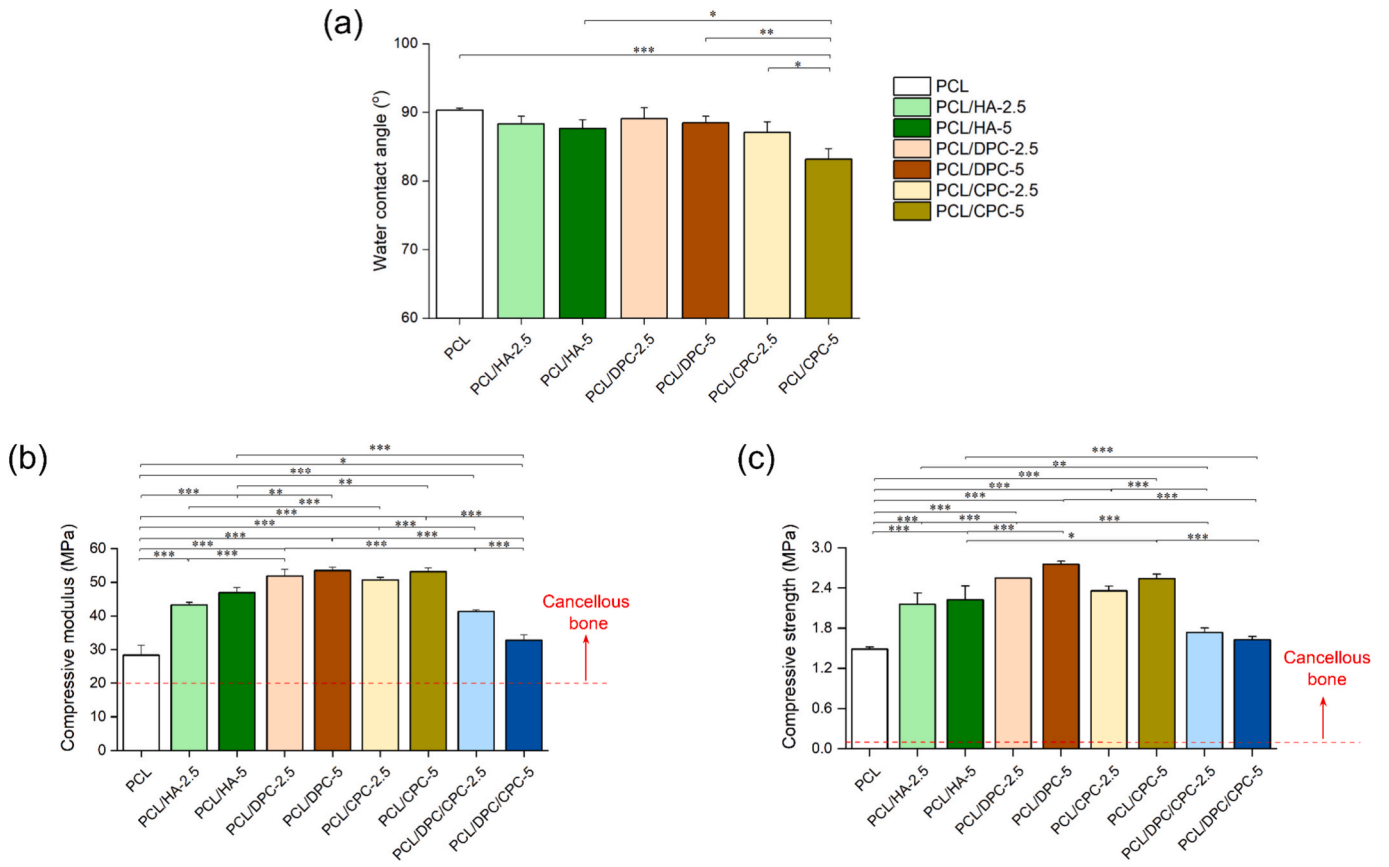

Fig. 3. Surface hydrophilicity and mechanical characterization results of all scaffolds. (a) WCA measurement. (b) compressive modulus, and (c) compressive strength. n = 3.

angle to 83.17 ± 1.55°, followed by 5 wt.% HA of 87.63 ± 1.31° and 5 wt.% DPC of 88.47 ± 0.97°. The obtained results are consistent with the findings from other researchers. Askarzadeh *et al.* incorporated BT into PVDF for the fabrication of piezoelectric scaffolds, which exhibited a reduced water contact angle compared to neat PVDF scaffolds [23]. Similarly, Zimina *et al.* investigated PLA/HA scaffolds and found that the addition of HA also decreased the WCA of the scaffolds [44]. Generally speaking, the increase of hydrophilicity with the induction of functional fillers could be due to the existence of ceramic on the polymer fibre surface, changing the surface morphology, and both CPC and DPC present stronger effects compared with HA [45]. With the same agglomerate size (the agglomerate size of both CPC and DPC is around 8——10 μm, as measured by SEM (Fig. S3) with the previously reported methodology [28]) and the same wt.%, the difference between CPC and DPC is minor; only 5 wt.% showed a significant difference. This could be due to the materials having similar adsorption capacity for water molecules [9,46], while the dose-dependent increase of hydrophilicity could be attributed to the hydrophilic nature of titania (TiO_2) in the ceramic composition [9]. Overall, the addition of ceramic-based functional fillers decreased the water contact angle by 7.93 % compared to the pure PCL scaffolds. The proposed method can be considered as a feasible dose-dependent approach to modulate the surface properties of BTE scaffolds.

3.2.2. *Mechanical characterization*

The mechanical properties of PCL scaffolds were significantly enhanced by incorporating the developed materials, as demonstrated in Fig. 3(b) and 3(c). Importantly, the results indicate that these scaffolds exhibit compressive strength and modulus values comparable to those of human cancellous bone (with compressive strength ranging from 0.1 to 16 MPa and modulus from 20 to 500 MPa, depending on the anatomical location) [47,48]. Moreover, the scaffolds are capable of enduring hydrostatic and pulse pressures typical of the physiological environment while maintaining the pores or spaces needed during the regeneration process [49,50]. Relating to the compressive modulus, DPC and CPC scaffolds showed a growing trend with the increase of DPC concentration (from 51.85 ± 1.94 MPa to 53.51 ± 0.94 MPa) and CPC (from 50.69 ± 0.79 MPa to 53.14 ± 1.1 MPa), while the PCL/HA scaffolds showed a similar trend (increase from 43.26 ± 0.78 to 46.91 ± 1.50 MPa). The superior mechanical properties of PCL/BNT scaffolds compared to PCL/HA scaffolds could be attributed to the inherent stiffness of the BNT piezoelectric ceramics, which is higher than HA [51,52]. BNT's Young's modulus (100–130 GPa) exceeds HA's (80–120 GPa), indicating greater stiffness, whereas BNT's compressive strength (400–800 MPa) surpasses HA's (100–500 MPa) significantly [51,52]. This increased rigidity allows for better stress distribution and absorption under compressive load [21]. Conversely, different from using a single material filler, PCL/DPC/CPC scaffolds presented a significantly decreasing trend (from 41.30 ± 0.49 to 32.79 ± 1.57 MPa) with concentration increasing. This is potentially due to the systematic error (including machine and operation) of the manufacturing process, such as fibre misalignment in the interface layer due to the shift when relocating the sample, which can be observed from Fig. S4. Under the same concentration, both the PCL/DPC and PCL/CPC scaffolds exhibited a significantly higher compressive modulus compared to the PCL/HA scaffold, whereas there was no statistical difference between the compressive modulus of PCL/DPC and PCL/CPC scaffolds. The enhancement effect on compressive modulus could potentially be attributed to the particles serving as strain absorbers within the polymeric matrix [53,54]. This is similar to the previous results of Mancuso *et al.* [22], who proved that the incorporation of piezoelectric ceramic particles (BT) into the polymeric matrix resulted in a composite structure exhibiting markedly enhanced mechanical performance in comparison to scaffolds composed of pure PCL and HA

composites [22]. Similarly, Zimina *et al.* also showed that the HA incorporation into the PLA enhanced the modulus and strength of the scaffolds [44].

The observed trends in compressive strength are similar to those of the compressive modulus, the PCL/DPC (from 2.54 ± 0.01 MPa to 2.76 ± 0.04 MPa), PCL/CPC (from 2.36 ± 0.07 MPa to 2.54 ± 0.07 MPa), and PCL/HA (from 2.15 ± 0.17 MPa to 2.22 ± 0.21 MPa) scaffolds, which slightly increased with material concentration. This is attributable to the uniform distribution of the ceramic phase within the polymer matrix and the intimate contact between the inorganic particles and the polymer matrix, which enhances the compressive strength of the composite scaffold [55–57]. However, the PCL/DPC/CPC scaffolds decreased (1.74 ± 0.07 to 1.63 ± 0.05 MPa) with increasing concentration of the materials, possibly due to a similar reason as described above. Overall, with the addition of the developed BNT functional fillers, the compressive modulus increased 88.6 % and compressive strength 85.4 % compared with neat PCL scaffolds. This dose-dependent moderation proved to be a viable approach to control and enhance the mechanical properties of the BTE scaffold.

3.3. In vitro biological characterization

3.3.1. Cell proliferation

Fig. 4(a) illustrates the cell viability and proliferation outcomes across all scaffolds. The fluorescence intensity, which directly correlates with the number of metabolically active cells, indicates that cell proliferation increased on all scaffolds from the time of seeding through day 7. Compared with the reference material scaffold (biocompatible and biodegradable PCL containing bio-ceramic HA), results demonstrate that the developed scaffolds have the ability to provide a favourable environment for cell proliferation with no significant cytotoxicity from the developed DPC and CPC. The hADSC proliferation status can also be observed in Fig. 4(b), 4(c), and 4(d), showing confluent cell bridging through the scaffold fibres.

Additionally, on both day 1 and day 3, no statistically significant differences were observed among the PCL/DPC, PCL/CPC, and PCL/HA scaffolds, with the exception that the PCL/DPC/CPC-2.5 scaffold exhibited significantly higher values than the PCL/HA-2.5 scaffold on day 3. This can be observed from Fig. S5, showing significantly more cells actin on the PCL/DPC/CPC scaffold than on the PCL/HA scaffold. Starting from day 5, the PCL/DPC and PCL/CPC scaffolds showed higher fluorescence intensity than the PCL/HA scaffolds at the same concentration. On day 7, the fluorescence intensity of the scaffolds with 5 wt.% DPC and CPC were significantly higher than scaffolds with the same concentration of HA or DPC/CPC, whereas there was no significant difference between DPC and CPC. All the mentioned results indicate that incorporating the developed piezoelectric ceramic materials enhances the proliferation of hADSCs. Although hybrid scaffolds (PCL/DPC/CPC) showed optimal results on day 1 and 3, from day 5 and onwards, PCL scaffolds containing a single type of piezoelectric material presented better results. Similar results to the above were obtained from an *in vitro* study by Mancuso *et al.* The incorporation of BT allowed the scaffolds to promote cell proliferation better than neat PCL and PCL/HA scaffolds [22]. Regardless of the hydrophilicity or the printing quality, the reason for this drop, particularly for PCL/DPC/CPC-5, could be due to either cell overconfluency or the change in the pH around the scaffold caused by ion release, such as Na^+, K^+, and Nb^+ from DPC and CPC [58,59]. The optimal pH for cell proliferation is usually between 7.0 and 7.2, a range that helps maintain normal metabolic and functional activity of cells, and deviations from this range may inhibit cell proliferation [54,60,61]. The released Na^+ ions may react with OH^- and raise the pH (alkaline tendency) around the scaffold [58,59]. Similarly, Kaviani *et al.* reported that the incorporation of forsterite core–shell nanoparticles elevated the pH around the scaffold and thus inhibited cell proliferation as the concentration of materials increased [54]. When applying a single functional filler in the scaffold, this effect could be minor. However, for the hybrid scaffold that contains both CPC and DPC, the combined effect due to different element compositions may inhibit cell proliferation at a later stage [62–64].

3.3.2. Osteogenic differentiation

hADSc osteogenic differentiation results are reported as ALP activity and ARS absorbance measurements, as illustrated in Fig. 5(a) and 5(b). ALP activity is an important factor for evaluating the calcium deposition and bone mineralization process [65], while ARS evaluates calcium-rich deposits by cells, reflecting osteogenesis-related activity [66,67]. The results indicate that all scaffolds effectively supported cell differentiation, and the incorporation of functional fillers significantly influenced both the ALP and ARS assay outcomes. Both results suggest a dose-dependent increase in the osteogenic differentiation behaviour, reflected by all the values increased from day 7 + 3 to day 7 + 14. However, the hybrid scaffold (PCL/DPC/CPC) consistently demonstrated the ability to promote osteogenic differentiation at the same level as the PCL/HA scaffold. For ARS, a similar trend was also observed, except the difference in values between the PCL/DPC and PCL/CPC scaffolds was not significant. Similar to ALP, the PCL/DPC/CPC and PCL/HA scaffolds exhibited significantly higher values compared to the PCL/DPC and PCL/CPC scaffolds, but notably, combining both piezoelectric materials in a single scaffold (PCL/DPC/CPC) seems to present higher results compared to PCL/HA scaffolds. Generally, in terms of promoting differentiation, considering a single type of piezoelectric ceramic material is less preferred compared with the hybrid approach (PCL/DPC/CPC scaffold). This may be because at the later stage of the cell culture, the alkaline pH around the scaffold caused by ions released from combining DPC and CPC promotes the osteogenic differentiation [62–64,68–70]. This is similar to the osteogenic process of bone constructs prepared from human bone marrow mesenchymal stem cells (hBMSC) combined with 45S5 bioactive glass (BG, a material that induces alkalinization of the external medium), evaluated by Monfoulet *et al.* [71]. Cell differentiation was positively affected in an alkaline environment. Therefore, while the initial alkaline shift may inhibit proliferation, it simultaneously creates a favourable environment for bone tissue regeneration at later stages.

The osteogenic differentiation results were further assessed through both confocal and SEM imaging. Confocal images (Fig. 5(c) and S6(a) illustrate the cell differentiation status at time points day 7 + 7 and 7 + 14. Confluent cells were growing on the scaffold, and bridging between fibres can be observed at day 7 + 14. SEM images captured at the same time point are presented in Fig. 5(d) and S6(b), with obvious calcium (Ca) deposition areas marked by red arrows. The corresponding EDX result also shows a significant peak for Ca (Fig. 5(g)), confirming the results. Additionally, all SEM images were further processed (Fig. 5(e)) for a semi-quantification of the mean area of calcium deposition per unit area (μm^2). The results (Fig. 5(f)) were well aligned with ARS results (Fig. 5(b)), indicating the superior differentiation result of the hybrid PCL/DPC/CPC-5 scaffold compared to the others. The obtained results echo a similar investigation from Jianqing *et al.*, who conducted an *in vivo* investigation of HA/BT scaffolds with the jawbone of a dog, and observed that HA/BT scaffolds significantly promoted osteogenesis compared to HA ceramics [72]. Similarly, Mancuso *et al.* also showed that BT piezoelectric ceramics outperformed HA in promoting cell differentiation [22]. However, the study of applying two piezoelectric ceramic materials (presenting direct and converse piezoelectric effects) is still limited.

4. Conclusions and future perspectives

This research developed two novel lead-free ceramic-based piezoelectric materials DPC and CPC (1-x) $Bi_{1/2}Na_{1/2}TiO_3$-x$KNbO_3$ (x = 0.01–0.09), and proposed a new type of 3D-printed porous BTE scaffolds considering both of them as functional fillers. Surface, mechanical, and *in vitro* biological properties were systematically evaluated,

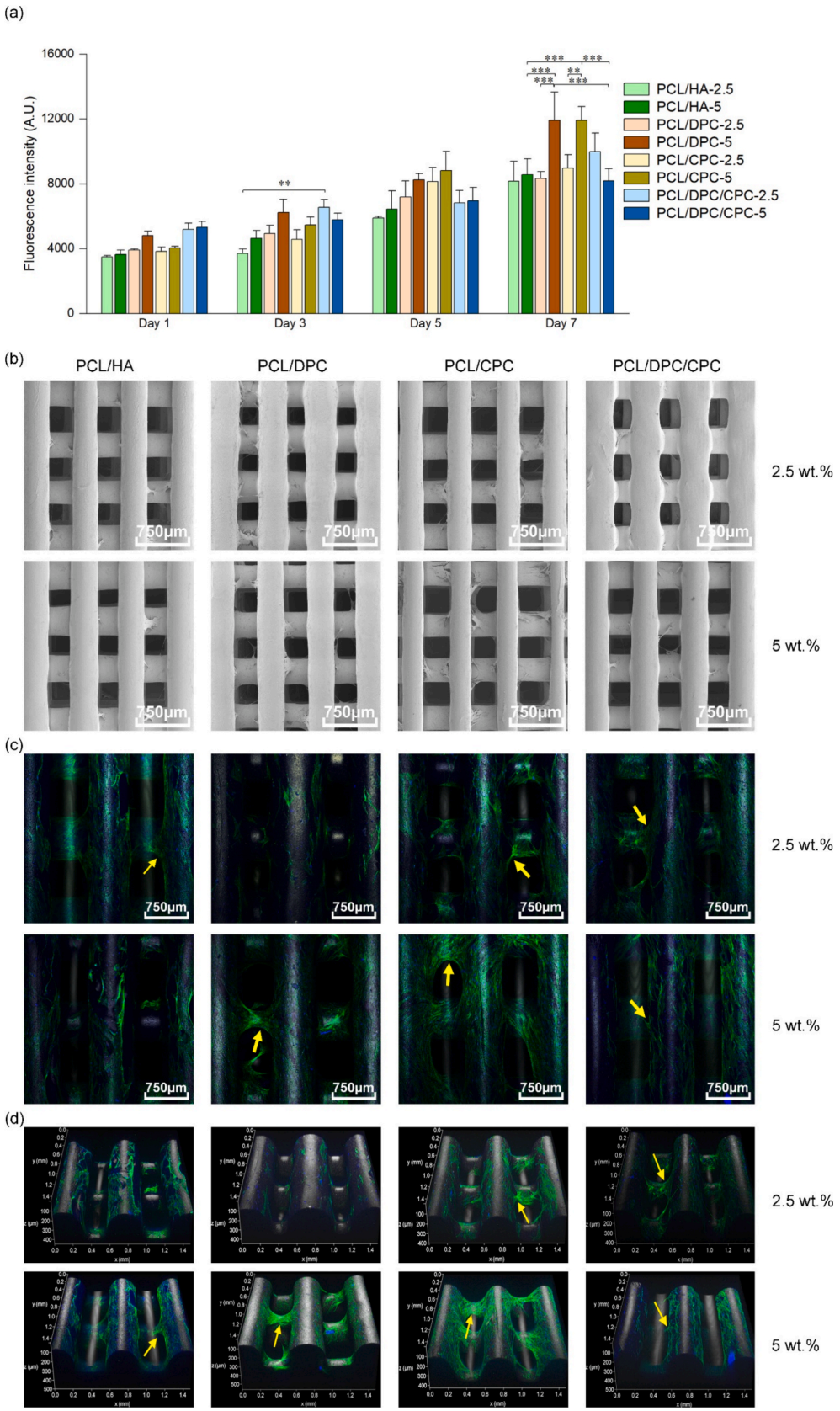

Fig. 4. Cell proliferation results on all types of scaffolds. (a) Fluorescence intensity measurement values at day 1, 3, 5 and 7; (b) SEM images of all cell-seeded scaffolds at day 7, showing cell growth and morphology on the scaffold fibre surfaces, and cell bridging between fibres. (c) 2D confocal and (d) 3D confocal microscopy images of all cell-seeded scaffolds at day 7. Cell nuclei stained blue and cellular actin stained green. Yellow arrows indicate cell bridging. n = 3. (For interpretation of the references to colour in this figure legend, the reader is referred to the web version of this article.)

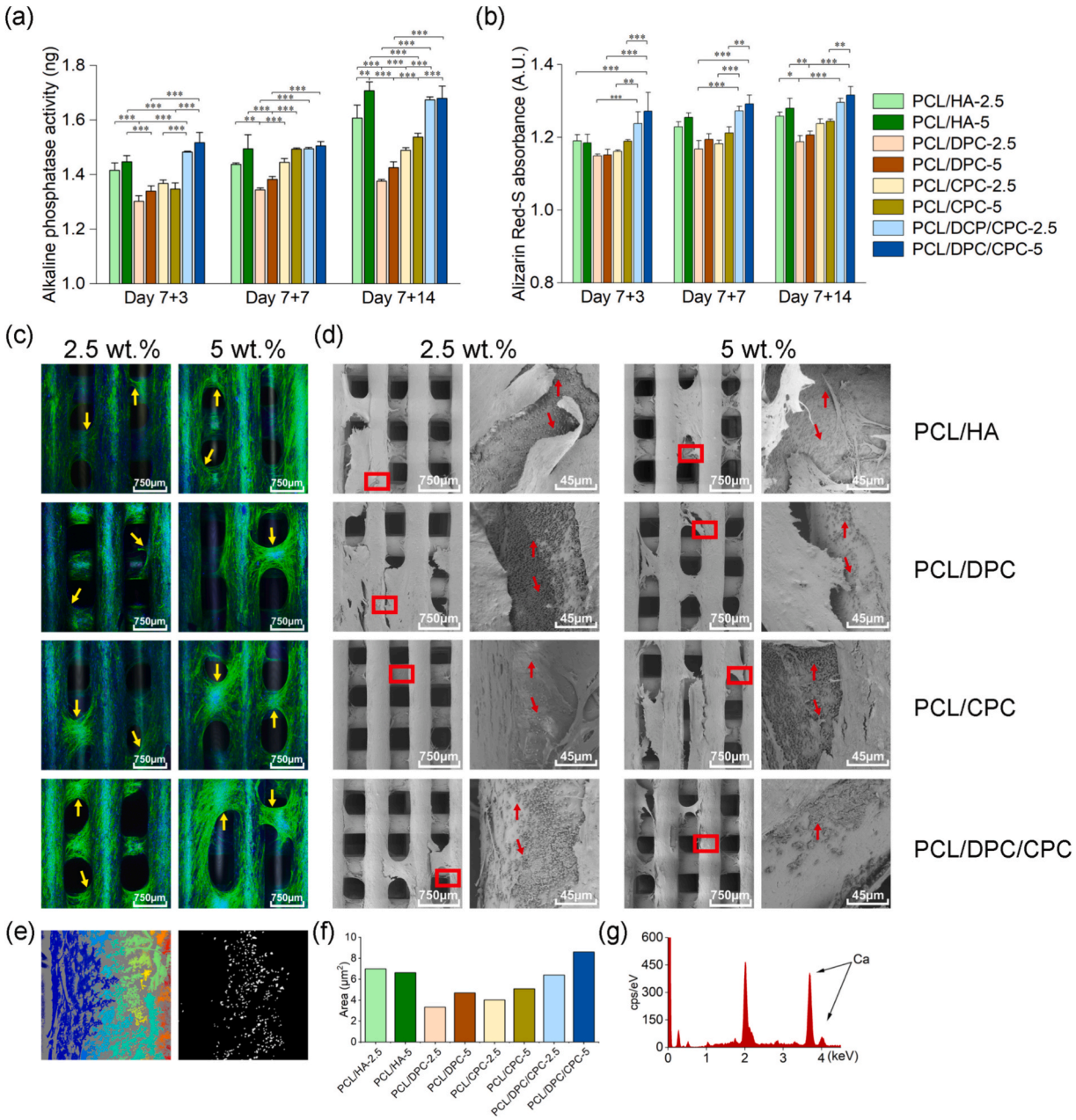

Fig. 5. Results of osteogenic differentiation of cells at time points day 7 + 3, day 7 + 7, and day 7 + 14. SEM and confocal images of all printed scaffolds at day 7 + 14. (a) ALP activity; (b) ARS absorbance; (c) confocal microscopy images (blue stained cell nuclei and green stained cellular actin); (d) SEM images; (e) RGB and extracted images of the calcium deposition area; (f) Calcium deposition semi-quantification result; and (g) mean area of calcium deposition on different scaffolds. Yellow arrows show cell bridges on the scaffold. Deposited calcium is shown by the red arrow. n = 3. (For interpretation of the references to colour in this figure legend, the reader is referred to the web version of this article.)

demonstrating that the incorporation of DPC and CPC significantly improved scaffolds mechanical performance (88.6 % enhancement of compressive modulus and 85.4 % enhancement of compressive strength compared to the neat PCL scaffold), closely aligning with the characteristics of human cancellous bone. The surface wettability of the scaffolds, as indicated by a 7.93 % reduction in water contact angle, was notably improved by the incorporation of both DPC and CPC, outperforming conventional PCL scaffolds. In vitro biological outcomes (including a 46.3 % improvement in cell proliferation and a 7.4 % improvement in osteogenic differentiation) demonstrated that the scaffolds incorporating both DPC and CPC outperformed PCL/HA scaffolds. All obtained results indicate that integrating DPC and CPC into 3D-printed scaffolds can enhance the mechanical and biological properties of the scaffolds, demonstrating their potential for BTE application.

Additionally, in terms of *in vitro* biological performance, researchers also found that using a single functional filler (DPC or CPC) typically promotes cell proliferation (a 45.6 % increase compared to PCL/DPC/CPC scaffolds), while the simultaneous use of two fillers (DPC and CPC) is more conducive to osteogenic differentiation (a 9.1 % increase compared to single-functional filler scaffolds).

While the experimental results are promising, further improvements are needed to enhance the performance of the proposed approach. From the materials perspective, lead-free piezoelectric materials offer significant potential, with direct (d_{33} > 200 pC/N) and/or large signal converse (d_{33}* >500 pm/V) piezoelectric performance. Future improvements will focus on compositions near the morphotropic phase boundary or those exhibiting phase transition behaviour, as these structures can enhance piezoelectric properties. A promising approach

involves designing a mixture of polar nanoregions and macroscopic long-range domains to achieve superior performance. The ion release during the potential material degradation process also deserves investigation. From the scaffold development perspective, it is essential to confirm the uniform distribution of piezoelectric ceramics within the scaffold through combined characterization techniques, including TGA, Raman spectroscopy, and transmission electron microscopy (TEM), since this uniformity is a key factor affecting scaffold performance. Increasing the concentration of piezoelectric ceramics also plays a critical role in enhancing scaffold piezoelectric activity. Optimisation factors such as particle size (ranging from nanometres to micrometres) and the porosity layout of 3D-printed scaffolds will be explored. The manufacturing processes and the unitarized system will be further improved to increase the as-fabricated scaffold quality. Furthermore, future research will also focus on developing advanced piezoelectric characterization techniques for porous 3D scaffolds and implementing dynamic cell culture methods that incorporate mechanical and electrical stimulation. Modelling and simulation approaches mimicking these dynamic testing methods will also be explored. During *in vitro* cell culture, it is important to investigate changes in the pH of the medium surrounding the scaffold with a customised sampling technique matching the porous scaffold architecture, contributing to accurate correlation with the obtained cell proliferation and differentiation result. Lastly, *in vivo* osteogenesis and degradation studies are critical steps to advance these scaffolds toward clinical applications. By addressing these challenges, this research paves the way for the systematic design of biomaterials tailored for specific tissue engineering applications, opening new possibilities in the field.

CRediT authorship contribution statement

Duo Meng: Writing – original draft, Visualization, Validation, Methodology, Investigation, Formal analysis, Data curation. **Yanhao Hou:** Writing – review & editing, Writing – original draft, Visualization, Validation, Methodology, Investigation, Formal analysis. **Hareem Zubairi:** Validation, Methodology, Investigation, Formal analysis. **Mustafa Tugrul Ucan:** Investigation. **David A Hall:** Writing – review & editing, Methodology. **Antonio Feteira:** Writing – review & editing, Methodology. **Paulo Bartolo:** Writing – review & editing. **Ge Wang:** Writing – review & editing, Writing – original draft, Supervision, Project administration, Funding acquisition, Conceptualization. **Weiguang Wang:** Writing – review & editing, Writing – original draft, Supervision, Project administration, Funding acquisition, Conceptualization.

Declaration of competing interest

The authors declare that they have no known competing financial interests or personal relationships that could have appeared to influence the work reported in this paper.

Acknowledgements

The authors wish to acknowledge Rosetrees Trust UK for the Continuation Funding (Ref: CF-2023-I-2\103). The authors also gratefully acknowledge the support of the Dame Kathleen Ollerenshaw Fellowship and Dean's PhD Scholarship provided by The University of Manchester. G.W. also acknowledges the support from Royal Society of Chemistry research fund (R23-5982928392).

Appendix A. Supplementary data

Supplementary data to this article can be found online at https://doi.org/10.1016/j.matdes.2025.114542.

Data availability

Data will be made available on request.

References

[1] Y. Hou, W. Wang, P. Bartolo, Application of additively manufactured 3D scaffolds for bone cancer treatment: a review, Bio-Des. Manuf. 5 (2022) 556–579, https://doi.org/10.1007/s42242-022-00182-7.
[2] W. Wang, J.R.P. Junior, P.R.L. Nalesso, D. Musson, J. Cornish, F. Mendonça, G. F. Caetano, P. Bártolo, Engineered 3D printed poly(ε-caprolactone)/graphene scaffolds for bone tissue engineering, Mater. Sci. Eng. C 100 (2019) 759–770, https://doi.org/10.1016/j.msec.2019.03.047.
[3] G.L. Koons, M. Diba, A.G. Mikos, Materials design for bone-tissue engineering, Nat. Rev. Mater. 5 (2020) 584–603, https://doi.org/10.1038/s41578-020-0204-2.
[4] X. Zhang, T. Wang, Z. Zhang, H. Liu, L. Li, A. Wang, J. Ouyang, T. Xie, L. Zhang, J. Xue, W. Tao, Electrical stimulation system based on electroactive biomaterials for bone tissue engineering, Mater. Today (2023) S1369702123002043, https://doi.org/10.1016/j.mattod.2023.06.011.
[5] B. Reid, M. Zhao, The Electrical Response to Injury: Molecular Mechanisms and Wound Healing, Adv. Wound Care 3 (2014) 184–201, https://doi.org/10.1089/wound.2013.0442.
[6] N. Goonoo, A. Bhaw-Luximon, Piezoelectric polymeric scaffold materials as biomechanical cellular stimuli to enhance tissue regeneration, Mater. Today Commun. 31 (2022) 103491, https://doi.org/10.1016/j.mtcomm.2022.103491.
[7] A. Wang, Z. Liu, M. Hu, C. Wang, X. Zhang, B. Shi, Y. Fan, Y. Cui, Z. Li, K. Ren, Piezoelectric nanofibrous scaffolds as in vivo energy harvesters for modifying fibroblast alignment and proliferation in wound healing, Nano Energy 43 (2018) 63–71, https://doi.org/10.1016/j.nanoen.2017.11.023.
[8] M. Zarei, A. Samimi, M. Khorram, M.M. Abdi, S.I. Golestaneh, Fabrication and characterization of conductive polypyrrole/chitosan/collagen electrospun nanofiber scaffold for tissue engineering application, Int. J. Biol. Macromol. 168 (2021) 175–186, https://doi.org/10.1016/j.ijbiomac.2020.12.031.
[9] N. Peidavosi, M. Azami, N. Beheshtizadeh, A., Ramazani Saadatabadi, Piezoelectric conductive electrospun nanocomposite PCL/Polyaniline/Barium Titanate scaffold for tissue engineering applications, Sci. Rep. 12 (2022) 20828, https://doi.org/10.1038/s41598-022-25332-w.
[10] D. Meng, Y. Hou, D. Kurniawan, R.-J. Weng, W.-H. Chiang, W. Wang, 3D-printed Graphene and Graphene Quantum Dot-Reinforced Polycaprolactone Scaffolds for Bone-Tissue Engineering, ACS Appl. Nano Mater. 7 (2024) 1245–1256, https://doi.org/10.1021/acsanm.3c05225.
[11] M.A. Marsudi, R.T. Ariski, A. Wibowo, G. Cooper, A. Barlian, R. Rachmantyo, P.J. D.S. Bartolo, Conductive Polymeric-based Electroactive Scaffolds for Tissue Engineering applications: Current Progress and challenges from Biomaterials and Manufacturing Perspectives, IJMS 22 (2021) 11543, https://doi.org/10.3390/ijms222111543.
[12] D. Khare, Electrical stimulation and piezoelectric biomaterials for bone tissue engineering applications, (2020).
[13] B. Tandon, J.J. Blaker, S.H. Cartmell, Piezoelectric materials as stimulatory biomedical materials and scaffolds for bone repair, Acta Biomater. 73 (2018) 1–20, https://doi.org/10.1016/j.actbio.2018.04.026.
[14] J. Jacob, N. More, K. Kalia, G. Kapusetti, Piezoelectric smart biomaterials for bone and cartilage tissue engineering, Inflamm Regener 38 (2018) 2, https://doi.org/10.1186/s41232-018-0059-8.
[15] K. Chen, X. Sun, M. Zhang, S. Zheng, C. Zou, L. Wang, Y. Liu, H. Tang, H. Zheng, C. Wang, X. Yu, F. Wang, G. Wu, 3D printed bismuth sodium titanate/hydroxyapatite piezoelectric ceramics: as an alternative material for bone repair, Mater. Today Commun. 44 (2025) 112179, https://doi.org/10.1016/j.mtcomm.2025.112179.
[16] C. Polley, T. Distler, R. Detsch, H. Lund, A. Springer, A.R. Boccaccini, H. Seitz, 3D Printing of Piezoelectric Barium Titanate-Hydroxyapatite Scaffolds with Interconnected Porosity for Bone Tissue Engineering, Materials 13 (2020) 1773, https://doi.org/10.3390/ma13071773.
[17] T. Tariverdian, A. Behnamghader, P. Brouki Milan, H. Barzegar-Bafrooei, M. Mozafari, 3D-printed barium strontium titanate-based piezoelectric scaffolds for bone tissue engineering, Ceram. Int. 45 (2019) 14029–14038, https://doi.org/10.1016/j.ceramint.2019.04.102.
[18] X. Yang, Y. Wang, Y. Zhou, J. Chen, Q. Wan, The Application of Polycaprolactone in Three-Dimensional Printing Scaffolds for Bone Tissue Engineering, Polymers 13 (2021) 2754, https://doi.org/10.3390/polym13162754.
[19] D. Rahmatabadi, M.A. Yousefi, S. Shamsolhodaei, M. Baniassadi, K. Abrinia, M. Bodaghi, M. Baghani, 4D Printing of Polyethylene Glycol-Grafted Carbon Nanotube-Reinforced polyvinyl Chloride–Polycaprolactone Composites for Enhanced Shape Recovery and Thermomechanical Performance, Adv. Intell. Syst. (2025) 2500113, https://doi.org/10.1002/aisy.202500113.
[20] D. Rahmatabadi, M. Aberoumand, K. Soltanmohammadi, E. Soleyman, I. Ghasemi, M. Baniassadi, K. Abrinia, M. Bodaghi, M. Baghani, 4D Printing-Encapsulated Polycaprolactone–Thermoplastic polyurethane with High Shape memory Performances, Adv. Eng. Mater. 25 (2023) 2201309, https://doi.org/10.1002/adem.202201309.
[21] R. Salehi Sadati, H. Eslami, M. Rafienia, M. Ansari, Piezo-biphasic scaffold based on polycaprolactone containing $BaTiO_3$ and hydroxyapatite nanoparticles using three-dimensional printing for bone regeneration, Int J Applied Ceramic Tech 22 (2025), https://doi.org/10.1111/ijac.14906.

[22] E. Mancuso, L. Shah, S. Jindal, C. Serenelli, Z.M. Tsikriteas, H. Khanbareh, A. Tirella, Additively manufactured BaTiO3 composite scaffolds: a novel strategy for load bearing bone tissue engineering applications, Mater. Sci. Eng. C 126 (2021) 112192, https://doi.org/10.1016/j.msec.2021.112192.

[23] N. Askarzadeh, Z. Sherafat, M. Sani, N. Azarpira, Development of Hybrid Polyvinylidene Fluoride-Barium Titanate/Polyvinyl Alcohol-Hydroxyapatite Co-Electrospun Piezoelectric Scaffold as a Stimulator for Bone Tissue Regeneration, Polymers for Advanced Techs 35 (2024), https://doi.org/10.1002/pat.70016.

[24] A. Standard, D1621; Standard Test Method for Compressive Properties of rigid Cellular Plastics, ASTM International: West Conshohocken, PA, USA, 2016.

[25] T. Fiedler, A.C. Videira, P. Bártolo, M. Strauch, G.E. Murch, J.M.F. Ferreira, On the mechanical properties of PLC–bioactive glass scaffolds fabricated via BioExtrusion, Mater. Sci. Eng. C 57 (2015) 288–293, https://doi.org/10.1016/j.msec.2015.07.063.

[26] W. Jo, S. Schaab, E. Sapper, L.A. Schmitt, H.-J. Kleebe, A.J. Bell, J. Rödel, On the phase identity and its thermal evolution of lead free (Bi1/2Na1/2)TiO3-6 mol% BaTiO3, J. Appl. Phys. 110 (2011) 074106, https://doi.org/10.1063/1.3645054.

[27] G. Wang, Z. Lu, Z. Zhang, Antonio. Feteira, C.C. Tang, D.A. Hall, Electric field-induced irreversible relaxor to ferroelectric phase transformations in Na $_{0.5}$ Bi $_{0.5}$ TiO $_3$ -NaNbO $_3$ ceramics, J Am Ceram Soc 102 (2019) 7746–7754. https://doi.org/10.1111/jace.16676.

[28] G. Wang, D.A. Hall, Y. Li, C.A. Murray, C.C. Tang, Structural characterization of the electric field-induced ferroelectric phase in Na0.5Bi0.5TiO3-KNbO3 ceramics, J. Eur. Ceram. Soc. 36 (2016) 4015–4021, https://doi.org/10.1016/j.jeurceramsoc.2016.06.022.

[29] G. Viola, R. MKinnon, V. Koval, A. Adomkevicius, S. Dunn, H. Yan, Lithium-Induced Phase Transitions in Lead-Free $Bi_{0.5}$ $Na_{0.5}$ TiO_3 Based Ceramics, J. Phys. Chem. C 118 (2014) 8564–8570. https://doi.org/10.1021/jp500609h.

[30] W. Jo, J.E. Daniels, J.L. Jones, X. Tan, P.A. Thomas, D. Damjanovic, J. Rödel, Evolving morphotropic phase boundary in lead-free (Bi1/2Na1/2)TiO3–BaTiO3 piezoceramics, J. Appl. Phys. 109 (2011) 014110, https://doi.org/10.1063/1.3530737.

[31] J. Wu, D. Xiao, J. Zhu, Potassium–sodium niobate lead-free piezoelectric materials: past, present, and future of phase boundaries, Chem. Rev. 115 (2015) 2559–2595.

[32] X. Zhao, C. Li, Y. Wang, W. Han, Y. Yang, Hybridized nanogenerators for effectively scavenging mechanical and solar energies, iScience 24 (2021) 102415. https://doi.org/10.1016/j.isci.2021.102415.

[33] G. Wang, Y. Li, C.A. Murray, C.C. Tang, D.A. Hall, Thermally-induced phase transformations in Na $_{0.5}$ Bi $_{0.5}$ TiO $_3$ –KNbO $_3$ ceramics, J Am Ceram Soc 100 (2017) 3293–3304, https://doi.org/10.1111/jace.14856.

[34] W. Jo, R. Dittmer, M. Acosta, J. Zang, C. Groh, E. Sapper, K. Wang, J. Rödel, Giant electric-field-induced strains in lead-free ceramics for actuator applications – status and perspective, J. Electroceram. 29 (2012) 71–93, https://doi.org/10.1007/s10832-012-9742-3.

[35] P. Shi, T. Li, X. Zhu, W. Liu, Q. Liu, B. Yang, X. Wang, R. Kang, S. Yang, X. Lou, High strain in Bi0.5Na0.5TiO3-based relaxors by adding two modifiers featuring with morphotropic phase boundary, Scripta Materialia 218 (2022) 114674, https://doi.org/10.1016/j.scriptamat.2022.114674.

[36] S. Kim, H. Nam, I. Calisir, Lead-free BiFeO3-based piezoelectrics: a review of controversial issues and current research state, Materials 15 (2022) 4388.

[37] M. Acosta, N. Novak, V. Rojas, S. Patel, R. Vaish, J. Koruza, G. Rossetti, J. Rödel, BaTiO3-based piezoelectrics: Fundamentals, current status, and perspectives, Appl. Phys. Rev. 4 (2017).

[38] J. Liu, H. Gu, Q. Liu, L. Ren, G. Li, An intelligent material for tissue reconstruction: the piezoelectric property of polycaprolactone/barium titanate composites, Mater. Lett. 236 (2019) 686–689.

[39] C. Shuai, G. Liu, Y. Yang, W. Yang, C. He, G. Wang, Z. Liu, F. Qi, S. Peng, Functionalized BaTiO3 enhances piezoelectric effect towards cell response of bone scaffold, Colloids Surf. B Biointerfaces 185 (2020) 110587, https://doi.org/10.1016/j.colsurfb.2019.110587.

[40] S.M. Oliveira, N.M. Alves, J.F. Mano, Cell interactions with superhydrophilic and superhydrophobic surfaces, J. Adhes. Sci. Technol. 28 (2014) 843–863, https://doi.org/10.1080/01694243.2012.697776.

[41] Y. Arima, H. Iwata, Effect of wettability and surface functional groups on protein adsorption and cell adhesion using well-defined mixed self-assembled monolayers, Biomaterials 28 (2007) 3074–3082, https://doi.org/10.1016/j.biomaterials.2007.03.013.

[42] P.B. Van Wachem, A.H. Hogt, T. Beugeling, J. Feijen, A. Bantjes, J.P. Detmers, W. G. Van Aken, Adhesion of cultured human endothelial cells onto methacrylate polymers with varying surface wettability and charge, Biomaterials 8 (1987) 323–328, https://doi.org/10.1016/0142-9612(87)90001-9.

[43] P.B. Van Wachem, T. Beugeling, J. Feijen, A. Bantjes, J.P. Detmers, W.G. Van Aken, Interaction of cultured human endothelial cells with polymeric surfaces of different wettabilities, Biomaterials 6 (1985) 403–408, https://doi.org/10.1016/0142-9612(85)90101-2.

[44] A. Zimina, F. Senatov, R. Choudhary, E. Kolesnikov, N. Anisimova, M. Kiselevskiy, P. Orlova, N. Strukova, M. Generalova, V. Manskikh, A. Gromov, A. Karyagina, Biocompatibility and Physico-Chemical Properties of Highly Porous PLA/HA Scaffolds for Bone Reconstruction, Polymers 12 (2020) 2938, https://doi.org/10.3390/polym12122938.

[45] S. Marecik, I. Pudełko-Prażuch, M. Balasubramanian, S.M. Ganesan, S. Chatterjee, K. Pielichowska, R. Kandaswamy, E. Pamuła, Effect of the Addition of Inorganic Fillers on the Properties of Degradable Polymeric Blends for Bone Tissue Engineering, Molecules 29 (2024) 3826, https://doi.org/10.3390/molecules29163826.

[46] S. Pramanik, P. Agarwala, K. Vasudevan, K. Sarkar, Human-lymphocyte cell friendly starch–hydroxyapatite biodegradable composites: Hydrophilic mechanism, mechanical, and structural impact, J of Applied Polymer Sci 137 (2020) 48913, https://doi.org/10.1002/app.48913.

[47] M. Dziaduszewska, A. Zieliński, Structural and Material Determinants Influencing the Behavior of Porous Ti and its Alloys made by Additive Manufacturing Techniques for Biomedical applications, Materials 14 (2021) 712, https://doi.org/10.3390/ma14040712.

[48] L.-C. Gerhardt, A.R. Boccaccini, Bioactive Glass and Glass-Ceramic Scaffolds for Bone Tissue Engineering, Materials 3 (2010) 3867–3910, https://doi.org/10.3390/ma3073867.

[49] S. Chung, M.W. King, Design concepts and strategies for tissue engineering scaffolds, Biotechnol. Appl. Biochem. 58 (2011) 423–438, https://doi.org/10.1002/bab.60.

[50] M. Mohammadi Zerankeshi, R. Bakhshi, R. Alizadeh, Polymer/metal composite 3D porous bone tissue engineering scaffolds fabricated by additive manufacturing techniques: a review, Bioprinting 25 (2022) e00191, https://doi.org/10.1016/j.bprint.2022.e00191.

[51] J. Chevalier, L. Gremillard, Ceramics for medical applications: a picture for the next 20 years, J. Eur. Ceram. Soc. 29 (2009) 1245–1255, https://doi.org/10.1016/j.jeurceramsoc.2008.08.025.

[52] P. Ramesh Babu, R. Selvamani, G. Singh, S. Kalainathan, R. Babu, V.S. Tiwari, Growth, mechanical and domain structure studies of Na0.5Bi0.5TiO3 single crystal grown by flux growth method, Journal of Alloys and Compounds 721 (2017) 199–204, https://doi.org/10.1016/j.jallcom.2017.05.318.

[53] A. Ali, A. Andriyana, Properties of multifunctional composite materials based on nanomaterials: a review, RSC Adv. 10 (2020) 16390–16403, https://doi.org/10.1039/C9RA10594H.

[54] Y. Kaviani, H. Eslami, M. Ansari, S.A. Poursamar, 3D printed magnetoactive nanocomposite scaffolds for bone regeneration, Biomed. Mater. 20 (2025) 015028, https://doi.org/10.1088/1748-605x/ad9f04.

[55] L. Chen, D. Zhai, C. Wu, J. Chang, Poly(d, l-lactic)-reinforced akermanite bioceramic scaffolds: Preparation and characterization, Ceram. Int. 40 (2014) 12765–12775, https://doi.org/10.1016/j.ceramint.2014.04.130.

[56] Y. Deng, M. Zhang, X. Chen, X. Pu, X. Liao, Z. Huang, G. Yin, A novel akermanite/poly (lactic-co-glycolic acid) porous composite scaffold fabricated via a solvent casting-particulate leaching method improved by solvent self-proliferating process, Regener. Biomater. 4 (2017) 233–242, https://doi.org/10.1093/rb/rbx014.

[57] A. Jadidi, E. Salahinejad, Mechanical strength and biocompatibility of bredigite (Ca7MgSi4O16) tissue-engineering scaffolds modified by aliphatic polyester coatings, Ceram. Int. 46 (2020) 16439–16446, https://doi.org/10.1016/j.ceramint.2020.03.206.

[58] C. Vitale-Brovarone, E. Verné, L. Robiglio, P. Appendino, F. Bassi, G. Martinasso, G. Muzio, R. Canuto, Development of glass–ceramic scaffolds for bone tissue engineering: Characterisation, proliferation of human osteoblasts and nodule formation, Acta Biomater. 3 (2007) 199–208, https://doi.org/10.1016/j.actbio.2006.07.012.

[59] W. Liu, X. Dan, W.W. Lu, H. Pan, Importance of Biomaterials In Vivo Microenvironment pH (μe-pH) in the Regeneration Process of Osteoporotic Bone Defects, in: C. Liu, H. He (Eds.), Developments and Applications of Calcium Phosphate Bone Cements, Springer Singapore, Singapore, 2018: pp. 473–495. https://doi.org/10.1007/978-981-10-5975-9_11.

[60] C.R. Kruse, M. Singh, S. Targosinski, I. Sinha, J.A. Sørensen, E. Eriksson, K. Nuutila, The effect of pH on cell viability, cell migration, cell proliferation, wound closure, and wound reepithelialization: In vitro and in vivo study, Wound Repair Regeneration 25 (2017) 260–269, https://doi.org/10.1111/wrr.12526.

[61] M. Flinck, S.H. Kramer, S.F. Pedersen, Roles of pH in control of cell proliferation, Acta Physiol. 223 (2018) e13068, https://doi.org/10.1111/apha.13068.

[62] C. Shuai, Z. Wang, H. Zhang, J. Jia, L. Huang, D. Wang, S. Chen, P. Feng, Biosoluble ceramic fiber reinforced poly(L-lactic acid) bone scaffold: degradation and bioactivity, npj Mater. Degrad. 6 (2022) 87, https://doi.org/10.1038/s41529-022-00297-3.

[63] Z. Lin, J. Wu, W. Qiao, Y. Zhao, K.H.M. Wong, P.K. Chu, L. Bian, S. Wu, Y. Zheng, K.M.C. Cheung, F. Leung, K.W.K. Yeung, Precisely controlled delivery of magnesium ions thru sponge-like monodisperse PLGA/nano-MgO-alginate core-shell microsphere device to enable in-situ bone regeneration, Biomaterials 174 (2018) 1–16, https://doi.org/10.1016/j.biomaterials.2018.05.011.

[64] U. Paik, S. Lee, V.A. Hackley, Influence of Barium Dissolution on the Electrokinetic Properties of Colloidal $BaTiO_3$ in an Aqueous Medium, J. Am. Ceram. Soc. 86 (2003) 1662–1668, https://doi.org/10.1111/j.1151-2916.2003.tb03537.x.

[65] S. Ansari, K. Ito, S. Hofmann, Alkaline Phosphatase activity of Serum Affects Osteogenic Differentiation Cultures, ACS Omega 7 (2022) 12724–12733, https://doi.org/10.1021/acsomega.1c07225.

[66] H. Puchtler, S.N. Meloan, M.S. Terry, ON THE HISTORY AND MECHANISM OF ALIZARIN AND ALIZARIN RED S STAINS FOR CALCIUM, J. Histochem. Cytochem. 17 (1969) 110–124, https://doi.org/10.1177/17.2.110.

[67] A. Bernar, J.V. Gebetsberger, M. Bauer, W. Streif, M. Schirmer, Optimization of the Alizarin Red S Assay by Enhancing Mineralization of Osteoblasts, IJMS 24 (2022) 723, https://doi.org/10.3390/ijms24010723.

[68] Y. Shen, W. Liu, C. Wen, H. Pan, T. Wang, B.W. Darvell, W.W. Lu, W. Huang, Bone regeneration: importance of local pH—strontium-doped borosilicate scaffold, J. Mater. Chem. 22 (2012) 8662, https://doi.org/10.1039/c2jm16141a.

[69] W. Liu, T. Wang, C. Yang, B.W. Darvell, J. Wu, K. Lin, J. Chang, H. Pan, W.W. Lu, Alkaline biodegradable implants for osteoporotic bone defects—importance of microenvironment pH, Osteoporos Int. 27 (2016) 93–104, https://doi.org/10.1007/s00198-015-3217-8.

[70] Y. Shen, W. Liu, K. Lin, H. Pan, B.W. Darvell, S. Peng, C. Wen, L. Deng, W.W. Lu, J. Chang, Interfacial pH: a critical factor for Osteoporotic Bone Regeneration, Langmuir 27 (2011) 2701–2708, https://doi.org/10.1021/la104876w.
[71] L.-E. Monfoulet, P. Becquart, D. Marchat, K. Vandamme, M. Bourguignon, E. Pacard, V. Viateau, H. Petite, D. Logeart-Avramoglou, The pH in the microenvironment of human mesenchymal stem cells is a critical factor for optimal osteogenesis in tissue-engineered constructs, Tissue Eng. A 20 (2014) 1827–1840, https://doi.org/10.1089/ten.tea.2013.0500.
[72] F. Jianqing, Y. Huipin, Z. Xingdong, Promotion of Osteogenesis by a Piezoelectric Biological Ceramic 18 (1997).